

Research on Engineering Structures & Materials



www.jresm.org



Experimental and predictive assessment of recycled rubber-modified lightweight mortars

Luma Ahmed Aday

Online Publication Date: 10 September 2025

URL: http://www.jresm.org/archive/resm2025-1063ma0807rs.html

DOI: http://dx.doi.org/10.17515/resm2025-1063ma0807rs

Journal Abbreviation: Res. Eng. Struct. Mater.

To cite this article

Aday L A. Experimental and predictive assessment of recycled rubber-modified lightweight mortars. *Res. Eng. Struct. Mater.*, 2025; 11(5): 2681-2699.

Disclaimer

All the opinions and statements expressed in the papers are on the responsibility of author(s) and are not to be regarded as those of the journal of Research on Engineering Structures and Materials (RESM) organization or related parties. The publishers make no warranty, explicit or implied, or make any representation with respect to the contents of any article will be complete or accurate or up to date. The accuracy of any instructions, equations, or other information should be independently verified. The publisher and related parties shall not be liable for any loss, actions, claims, proceedings, demand or costs or damages whatsoever or howsoever caused arising directly or indirectly in connection with use of the information given in the journal or related means.



Published articles are freely available to users under the terms of Creative Commons Attribution - NonCommercial 4.0 International Public License, as currently displayed at here (the "CC BY - NC").



Research on Engineering Structures & Materials



www.jresm.org

Research Article

Experimental and predictive assessment of recycled rubbermodified lightweight mortars

Luma Ahmed Aday *,a

Civil Engineering Department, College of Engineering, Al-Iraqia University, Baghdad, Iraq

Article Info

Article History:

Received 07 Aug 2025 Accepted 17 Sep 2025

Keywords:

Rubberized lightweight concrete; Compressive strength prediction; Physical and mechanical properties; Artificial neural network

Abstract

This study examines lightweight cement mortars reinforced with Polyvinyl Alcohol (PVA) fibers to elucidate how introducing recycled rubber as a sand replacement influences microstructure-sensitive transport and load-bearing behavior. Using a standardized mix with a binary pozzolanic binder (Class F fly ash and silica fume), we assessed compressive and flexural strength, elastic modulus, stressstrain response, dry density, water absorption, and Ultrasonic Pulse Velocity (UPV). Increasing rubber fraction generally reduced strength and stiffness due to weaker interfacial bonding and elevated internal porosity; nevertheless, mortars with moderate rubber contents retained adequate strength while exhibiting enhanced plasticity/ductility, indicating potential for semi-structural use when properly optimized. An artificial neural network that ingests rubber content, dry density, water absorption, and UPV predicted 28-day compressive strength with high fidelity ($R^2 = 0.94$; MSE = 0.72MPa²; MAPE = 1.87%), with *UPV* emerging as the most influential predictor. The combined experimental and data-driven findings provide non-destructive, UPV-anchored guidance for designing PVA-reinforced lightweight rubberized mortars for sustainable construction.

© 2025 MIM Research Group. All rights reserved.

1. Introduction

Lightweight concrete is characterized by its low density, typically less than 2000 kg/m³, which is achieved by replacing conventional aggregates with lightweight materials such as recycled tire rubber. This reduction in mass contributes to lowering structural loads while maintaining the required mechanical performance. According to the American Tire Manufacturers Association, more than 300 million tires are discarded annually in the United States, with global figures exceeding 1.5 billion tires [1]. This environmental concern, along with rapid urbanization, has made waste tire management a pressing issue, prompting researchers to explore the use of recycled tires as partial replacements for traditional aggregates, with the dual objective of reducing environmental impact and improving concrete performance. One study showed that optimizing Tire-Derived Aggregate Concrete (TDAC) through particle grading, NaOH treatment, Supplementary Cementitious Materials (*SCMs*), and fiber reinforcement led to a 75.4% increase in compressive strength and a 465.6% improvement in toughness [2]. Other findings highlighted that since concrete strength is one of the most important parameters affecting structural performance, pretreatment of rubber with NaOH and silica significantly enhanced compressive strength and abrasion resistance, reaching 61.5 MPa at 10% replacement compared to untreated rubber concrete [3].

*Corresponding author: eng-luma00@aliraqia.edu.iq

^aorcid.org/0000-0002-2689-4167

DOI: http://dx.doi.org/10.17515/resm2025-1063ma0807rs

Res. Eng. Struct. Mat. Vol. 11 Iss. 5 (2025) 2681-2699

Treated rubber (e.g., with NaOH or silane) maintained adequate compressive strength at up to 25% replacement. While replacing fine aggregate with rubber ash reduced flexural strength, the addition of rubber fibers improved mechanical properties and durability, as confirmed by microstructural analysis [4]. Furthermore, in addition, the incorporation of 1% rubber fibers by cement weight led to an improvement in compressive strength by 4.9% and flexural strength by 8.9%, while the splitting tensile strength decreased by approximately 12.4%. [5]. Rubberized concrete was also found to maintain acceptable strength levels up to 20% rubber content, although poor bonding with cement paste remains a challenge that warrants further investigation [6]. In contrast, rubberized concrete lost 54%–92% of its impact resistance and 21%–52% of its tensile strength when exposed to temperatures between 100-200 °C, with rubber chips performing better than crumb rubber [7]. The highest fracture resistance was observed at 30% RAP with 0% rubber, suggesting that rubber inclusion may not necessarily enhance fracture performance [8]. In another study, the addition of PVA fibers to rubberized concrete resulted in compressive strength of 49 MPa and improved durability [9]. Replacing fine aggregate with 5-15% recycled tire rubber or 35-100% expanded clay aggregates reduced density and strength while increasing porosity, with expanded clay performing better overall, making rubber more suitable for non-structural, ecofriendly applications [10]. Similarly, it was found that replacing fine aggregate with recycled rubber in self-compacting concrete performed better than coarse aggregate replacement [11]. It was also found that tire rubber can replace up to 7.5% of fine aggregate in M30 concrete without significantly affecting strength or durability [12], while improved durability was reported in aggressive environments at 2.5-7.5% rubber content due to reduced chloride penetration, acid attack, and strength loss [13]. Moreover, adding up to 10% rubber powder with a sand ratio of 33–36% improved impact resistance, noise reduction, and shrinkage behavior, although larger particle sizes and higher contents reduced strength and stiffness [14]. Treatment methods using silica fume and sulfuric acid significantly enhanced cement-rubber bonding in foam concrete, improving compressive strength by up to 56% [15]. Another study found that replacing coarse aggregate with 20% untreated rubber reduced compressive strength by 49%, but strength was restored to acceptable levels through compression casting using treated aggregates [16]. Combining NaOH-treated rubber with silica fume improved long-term durability and sustainability at 20–40% rubber content [17]. Studies [18,19] confirmed that adding fibers significantly enhances the mechanical and dynamic properties of rubberized concrete, helping to overcome the inherent strength limitations associated with rubber inclusion. High contents of crumb rubber (up to 40%) were found to significantly reduce strength by up to 50%; however, incorporating 0-5% treated rubber at a 0.4 water-cement ratio improved ductility by 86.2% and enhanced microstructural properties [20]. Low levels of fine (2-4 mm) or coarse (15 mm) rubber aggregates have been shown to enhance ductility and energy dissipation with minimal strength loss, making rubberized concrete a promising material for seismic and impact-resistant structures [21]. Additionally, concrete incorporating more than 80% crumb rubber exhibited reduced carbonation rates, while fiber-coated rubber (FCR) improved freeze-thaw and acid resistance by enhancing matrix cohesion [22]. Further, fiber-coated and polymer fiber-reinforced rubber concretes demonstrated enhanced durability and mechanical properties, although further research is needed to determine the optimal mix design [23]. Long-term performance improvements were also observed, including a 12% increase in compressive strength after 90 days [24]. While waste tire rubber typically reduces the mechanical strength of concrete, the use of appropriate treatment methods and moderate replacement ratios can significantly enhance both performance and sustainability [25]. Moreover, modifying rubberized concrete with 10% silica fume and 0.1% polypropylene fibers improved mechanical strength and microstructural integrity by reducing voids and limiting microcrack propagation [26]. These findings collectively provide dedicated support for the incorporation of recycled rubber in concrete, especially when combined with pozzolanic materials and fiber reinforcements. Recent advances in predictive modeling further support this direction. For instance, an ANN model accurately predicted the frost resistance of rubberized concrete (R²=0.9825) based on mix proportions, rubber content, and freezethaw cycles, using relative dynamic elastic modulus as the durability metric [27]. Similarly, replacing 6% of aggregates with recycled rubber improved flexibility and crack resistance while maintaining similar performance to conventional concrete [28]. Machine learning models have also proven effective in predicting the mechanical properties of rubberized concrete at 28 days [29]. An *ANN* model successfully predicted compressive strength using input parameters such as the water-to-cement ratio and granular skeleton, achieving a high correlation (up to 99.76%) and low error rates, potentially eliminating the need for extensive experimental testing. A broader comparative study [30] used *ANN*, Linear Regression (*LR*), Random Forest (RF), and M5P models to estimate the compressive strength of mortar modified with up to 7.5% crumb rubber, finding *ANN* to be the most accurate (R = 0.9998, RMSE \approx 0.21). Moreover, [31] developed a Deep Neural Network (DNN) model using a comprehensive database of rubberized concrete mixes, achieving a high predictive accuracy (R² \approx 0.99, RMSE < 0.13), outperforming traditional *ANN* and regression models.

In spite of all previous studies do not provide a systematic evaluation of lightweight mortars that pair sand-equivalent rubber (matched gradation and morphology to sand) with joint proportioning of SCMs, PVA fibers, and rubber under fixed mixing conditions thereby decoupling particle-size/surface effects from compositional effects across unexplored replacement ranges. This study addresses that gap by building response maps linking those joint proportions to mechanical and transport properties, UPV/NDT metrics, and ITZ features, delineating a balanced proportion window for practical and semi-structural applications and providing NDT-based mix guidance.

2. Methodology

2.1 Materials and Mix Design

This study endeavors to evaluate a series of lightweight concrete mixes to investigate the effects of replacing natural sand with Granulated Tire Rubber (GTR) on both mechanical performance and ultrasonic pulse transmission within a cementitious matrix. GTR was incorporated as a volumetric replacement for fine aggregate in incremental steps ranging from 0% to 30%, with a 5% increase in each mix. All concrete formulations were designed and tested according to ASTM C330/C330M [32] specifications, which define structural lightweight concrete as having a dry density less than 2000 kg/m³. To maintain consistent bonding properties in all mixes, Type I Ordinary Portland Cement (OPC), conforming to ASTM C150, was used. In addition, two pozzolanic materials Class F fly ash conforming to ASTM C618 and silica fume conforming to ASTM C1240, were incorporated to improve microstructure and reduce porosity in the Interfacial Transition Zone (ITZ). Specifically, 25% of the cement content was replaced with fly ash, while silica fume contributed 8%, reducing the effective cement content from 400 kg/m³ to 268 kg/m³. Despite these substitutions, the total binder content was maintained at 400 kg/m³, in line with ACI 211.2-98 [33]. properties of OPC, fly ash, and silica fume are summarized in Table 1.

Table 1. Physical and chemical properties of OPC, fly ash (FA), and silica fume

Property	Specific Gravity	SiO ₂ (%)	Al ₂ O ₃ (%)	Fe ₂ O ₃ (%)	CaO (%)	MgO (%)	SO ₃ (%)	LOI (%)	PAI at 7 days (%) (ASTM C311/C311 M)	Retained on 45 μm sieve (%)
OPC	3.15	20.5	4.8	3.2	63. 7	1.5	2.7	1.5	-	-
Fly Ash	2.30	53.2	23.5	9.5	4.9	1.2	0.5	1.9	85.7	27
Silica Fume	2.21	92.0	1.0	0.5	0.2	0.3	0.1	1.0	112	7

Note: Properties as provided by the suppliers

PVA fibers were added at a constant volume ratio of 2% to all mixes. The main properties of PVA fibers are given in Table 2. A high-range water-reducing admixture (HRWRA), compliant with ASTM C494 Type F, was used to maintain workability without changing the water content. A constant water-to-binder (w/b) ratio of 0.45 was also adopted for all mixes to ensure uniform hydration and comparability of test results. The recycled rubber was sourced from end-of-life vehicle tires and processed via mechanical shredding, magnetic separation, and sieving to produce clean, fine rubber granules. the recycled rubber particles ranged from 0.3 to 1.5 mm, which is comparable to the fine fraction of natural sand in terms of particle size distribution. Fig.1 displays the particle size distribution curves of both rubber and sand, demonstrating their comparable fineness and ensuring uniformity and reduced risk of segregation during mixing.

Table 2. Properties of polyvinyl alcohol (PVA) fibers

Length (mm)	Diameter (μm)	L/D	Density (g/cm³)	Tensile Strength (MPa)	Modulus of Elasticity (GPa)	Elongation (%)
6.0	42.0	142	1.28	1700.0	57.0	6.0

Note: Properties as provided by the suppliers

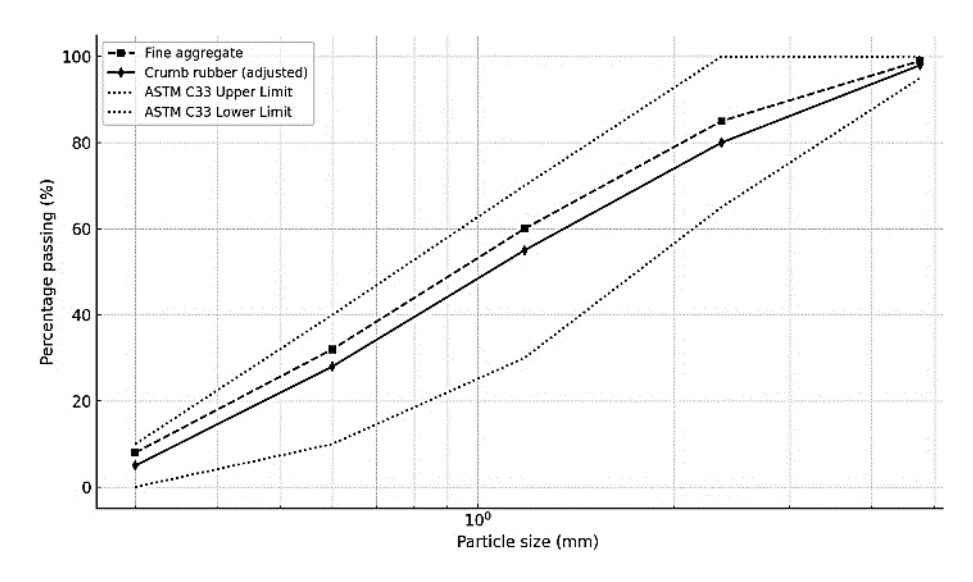


Fig. 1. Particle size distribution of fine aggregate and GTR with ASTM C33



Fig. 2. Recycled and pozzolanic materials used in rubberized mortar mixtures (a) PVA, (b) ground tire rubber, (c)silica fume, and (d) fly ash

Table 3. Mix proportions of mortar specimens with varying rubber powder replacement levels- m^3

Mix ID	Rubber Replacement (%)	OPC (kg/m³)	Fly Ash (kg/m³)	Silica Fume (kg/m³)	Water (kg/m³)	Superplasticizer %	Sand (kg/m³)	Rubber Powder (kg/m³)	<i>PVA</i> % Fibers
R0	0	268	100	32	0.45	1.2	850	0	2%
R5	5	268	100	32	0.45	1.2	807	47	2%
R10	10	268	100	32	0.45	1.2	765	94	2%
R15	15	268	100	32	0.45	1.2	723	141	2%
R20	20	268	100	32	0.45	1.2	680	188	2%
R25	25	268	100	32	0.45	1.2	638	235	2%
R30	30	268	100	32	0.45	1.2	595	282	2%

The rubber powder, with a specific gravity of approximately 1.10, exhibited an irregular shape and a soft, elastic surface texture. In contrast, the natural sand used had a specific gravity of about 2.62.

The proportions of the materials are summarized in Table 3. The materials are illustrated in (Fig 2.), which displays *PVA* fibers Fig. 2a, rubber granules Fig. 2b, silica fume Fig. 2c, and fly ash Fig. 2d.

2.2 Experimental Testing Program

An experimental program was designed to investigate the effect of Granulated Tire Rubber (GTR) on the mechanical and physical behavior of lightweight mortar. To ensure uniform dispersion of the components, a pan mixer was employed throughout the mixing process. The mixing procedure followed the guidelines of ASTM C192 with some modifications to accommodate the incorporation of rubber. The sequence consisted of dry mixing the natural aggregates and rubber particles for 1 minute, followed by the addition of cement, fly ash, and silica fume for another minute. Half of the mixing water was then introduced and mixing continued for 1 minute. Finally, the remaining water together with the High-Range Water-Reducing Admixture (HRWRA) was added, and mixing was extended for five minutes to obtain a homogeneous mixture.

The fresh mortar was cast into $50 \times 50 \times 50$ mm cubes for compressive strength, dry density, water absorption, and ultrasonic pulse velocity (UPV) tests. Prisms of $40 \times 40 \times 160$ mm were prepared for flexural strength tests, while cylinders of 100×200 mm were used for modulus of elasticity tests. All specimens were compacted using a vibration table to eliminate entrapped air and ensure consistency. After 24 hours of casting, the specimens were demolded and water-cured at $[23 \pm 2$ °C] until the designated testing ages; laboratory handling/conditioning was conducted at $[50 \pm 5\%$ RH] and $[23 \pm 2$ °C]. The compressive and flexural strength tests were performed using a universal testing machine with a maximum load capacity of 2000 kN.

The tests were conducted in accordance with the relevant standards: compressive strength (ASTM C109) at 28 and 90 days, flexural strength (ASTM C348), modulus of elasticity (ASTM C469), ultrasonic pulse velocity (ASTM C597), and dry density and water absorption (ASTM C642) at 28 days. To ensure statistical validity and reliability, the average values were calculated from three specimens for each test. The Fig. 3 illustrates the laboratory workflow for rubberized mortar.

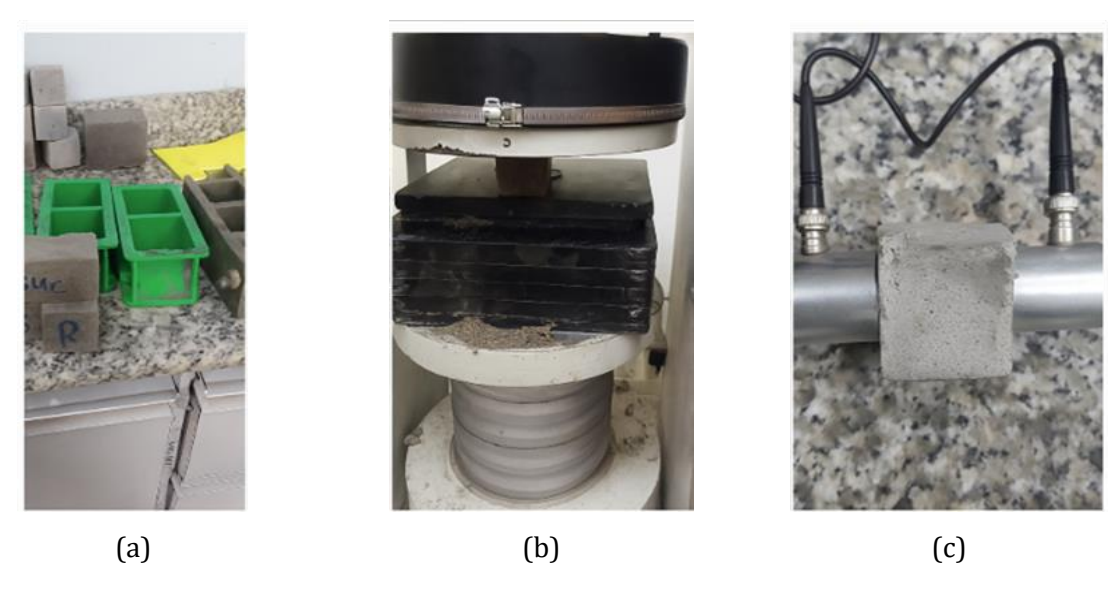


Fig. 3. Laboratory procedures for rubberized mortar testing

2.3 Prediction of Compressive Strength Using Artificial Neural Networks (ANN)

To complement the experimental results, a machine learning model was developed to explore the influence of selected physical parameters on the mechanical behavior of lightweight concrete using recycled rubber. This model utilized an *ANN* structured as a Multilayer Perceptron (*MLP*), with the primary objective of predicting the 28-day compressive strength. A notable advantage of this approach is its reliance on easily quantifiable input properties, reducing the need for repetitive and time-consuming laboratory tests. The *ANN* model was implemented using Python version 3.10 Supporting packages such as NumPy and Matplotlib were used to manage data preprocessing tasks

and facilitate graphical interpretation of the results. This predictive strategy provided a structured and efficient means of evaluating concrete performance based on experimental variables, complementing traditional testing procedures. The dataset contained 50 records. We randomly split the data into 70% training (n = 35), 15% validation (n = 8), and 15% testing (n = 7). The model relied on four input variables: *GTR* replacement ratio (%*GTR*), dry density, water absorption, and *UPV*. The network architecture consisted of three primary layers as shown in Fig. 4.

- Input Layer: Comprising four neurons representing the following input variables:
 - ➤ *GTR* replacement percentage (%Rubber)
 - > Dry density (kg/m³)
 - ➤ Water absorption (%)
 - Ultrasonic pulse velocity (UPV, km/s)
- Hidden Layers:
 - > The first hidden layer contains 8 neurons.
 - > The second hidden layer also contains 8 neurons.
 - The *ReLU* (Rectified Linear Unit) activation function was applied in both hidden layers to enhance the model's ability to learn nonlinear relationships.
- Output Layer: A single neuron was used to represent the predicted value of compressive strength (fc) in megapascals (MPa).

Prior to training, all variables were normalized using the Min–Max Scaling technique according to the following formula:

$$X = [x_{1}, x_{2}, x_{3}, x_{4}]^{T}$$
(1)

Where; x_1 : rubber content (%), x_2 : dry density (kg/m³), x_3 : water absorption (%), x_4 : ultrasonic pulse velocity (km/s).

Each feature was normalized using Min-Max scaling:

$$x_{i,norm}^{(n)} = \frac{x_i^{(n)} - x_{i,min}}{x_{i,max} - x_{i,min}} , \forall i = 1 \dots 4$$
 (2)

Where; $x_i^{(n)}$: the original value of feature i for sample n, $x_{i,min}$ and $x_{i,max}$: the minimum and maximum of feature i respectively. First hidden layer:

$$z_j^{(1)} = f\left(\sum_{i=1}^4 w_{ji}^{(1)} x_i + b_j^{(1)}\right), j = 1, 2, \dots, 8$$
(3)

Second hidden layer:

$$z_k^{(2)} = f\left(\sum_{j=1}^8 w_{kj}^{(2)} z_j^{(1)} + b_k^{(2)}\right), k = 1, 2, \dots, 8$$
(4)

Output layer:

$$\hat{\mathbf{y}} = \sum_{k=1}^{8} w_k^{(2)} z_k^{(3)} + b^{(3)}$$
 (5)

Where; w , b Weights and biases for layer, f: ReLU activation: f(x) = max(0, x) Training minimized the Mean Squared Error (MSE):

$$MSE = \frac{1}{N} \sum_{i=1}^{N} (y^{(i)} - \hat{y}^{(i)})^2$$
 (6)

Model accuracy was assessed using the coefficient of determination:

$$R^{2} = 1 - \frac{\sum_{i=1}^{N} (y^{(i)} - \hat{y}^{(i)})^{2}}{\sum_{i=1}^{N} (y^{(i)} - \overline{y})^{2}}$$

$$(7)$$

Where; y^i : actual value of sample I, \hat{y}^i : predicted value, \overline{y} : mean of actual values, N: number of samples.

The Mean Absolute Percentage Error (MAPE) was computed on the held-out test set:

$$MAPE \% = \sum_{i=1}^{N} \frac{100}{N} \left[\frac{\hat{y}^{(i)} - y^{(i)}}{y^{(i)}} \right]$$
 (8)

Training used Adam (learning rate = 1e-3) with a batch size of 16. Training ran for up to 5,000 epochs with early stopping (patience = 100) based on validation loss to mitigate overfitting. Hyperparameters were tuned on a held-out validation set via guided trial-and-error within reasonable bounds; the final configuration was selected by the minimum validation MSE

The outputs were inverse-transformed to their original scale:

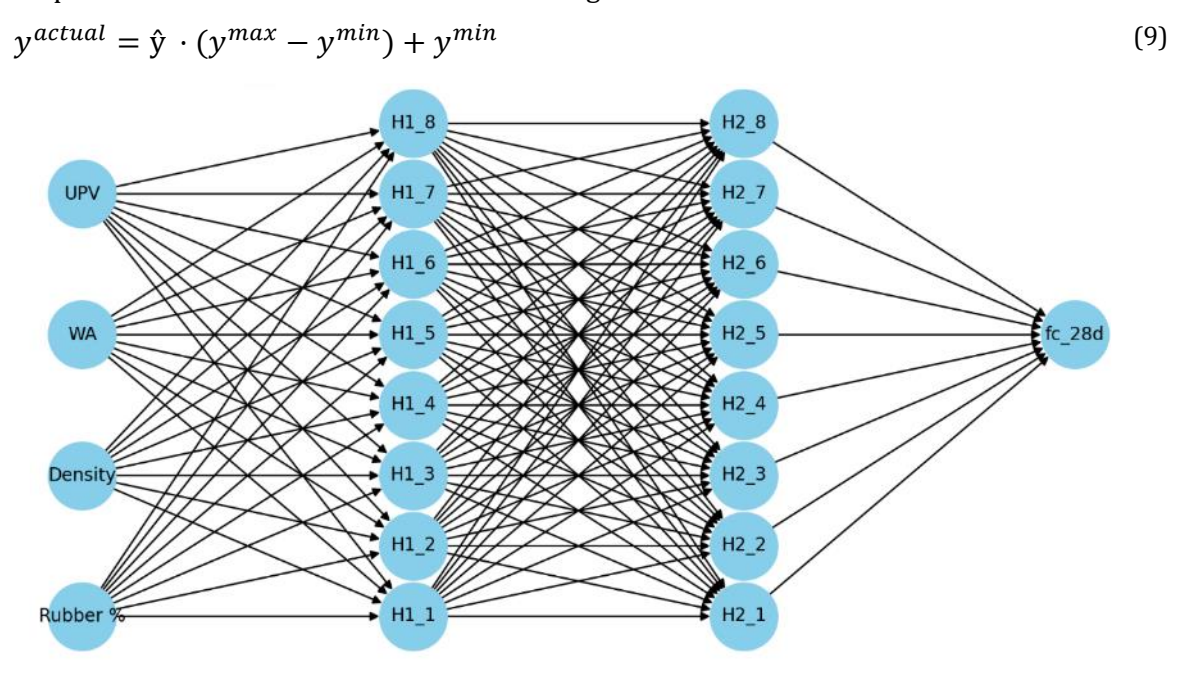


Fig. 4. Neural network architecture for predicting 28-day compressive strength

3. Result and Discussion

This section discusses the experimental results of the rubberized lightweight mortar mixtures, along with the predictive performance of the *ANN* model developed to estimate key mechanical parameters. The experimental tests provided a foundation for model training, and the *ANN*'s predictions were compared to the actual measured values to evaluate accuracy and generalization.

3.1 Compressive Strength Behavior

Compressive strength results at both 28 and 90 days including mean values, Standard Deviation (SD), and Coefficient of Variation (CoV) are presented in Table 4 and illustrated in Fig. 5. At 28 days, a progressive reduction in compressive strength was observed with increasing rubber powder replacement: approximately 14.5%, 23.8%, 31.2%, 40.0%, 48.1%, and 57.5% for R5–R30, respectively, compared to the reference mix R0. This trend is consistent with previous findings [39,40], which attributed the decline to the soft and hydrophobic nature of rubber particles that weaken the interfacial transition zone (ITZ), increase porosity, and reduce stiffness. Similarly, other studies [41,42] reported compromised mechanical performance due to weak rubber–cement bonding and

ineffective stress transfer across the matrix. Despite this strength degradation, CoV values for all mixes remained within the acceptable range of 4–6%, reflecting high internal consistency and effective compaction, supported by the use of HRWRA and well-dispersed PVA fibers. At 90 days, all mixes exhibited further strength gain over time. the reference mix R0 increased from 39.5 MPa at 28 days to 44.6 MPa at 90 days. Likewise, mix R5 improved from 33.8 to 40.4 MPa, R10 from 30.1 to 36.2 MPa, R15 from 27.2 to 33.1 MPa, R20 from 23.7 to 27.4 MPa, R25 from 20.5 to 21.9 MPa, and R30 from 16.8 to 19.2 MPa. This strength development is mainly attributed to the continuous hydration of unreacted cement particles, along with delayed pozzolanic reactions of fly ash and silica fume, which progressively consume calcium hydroxide and generate additional C–S–H gel. These secondary hydration products refine the pore structure, enhance the ITZ, and contribute to a denser microstructure, thereby improving long-term compressive strength. Nevertheless, the relative reductions compared to R0 at 90 days remained significant: 9.4% for R5, 18.9% for R10, 25.9% for R15, 38.5% for R20, 50.9% for R25, and 57.0% for R30.

These findings highlight a critical technical insight: although extended curing and refined mix design strategies particularly the inclusion of SCMs and PVA fibers can mitigate the negative effects of rubber inclusion to some extent, they cannot fully recover the structural integrity lost at higher rubber replacement levels. Thus, when incorporating recycled rubber into structural concrete, a careful balance must be maintained between sustainability goals and structural performance requirements.

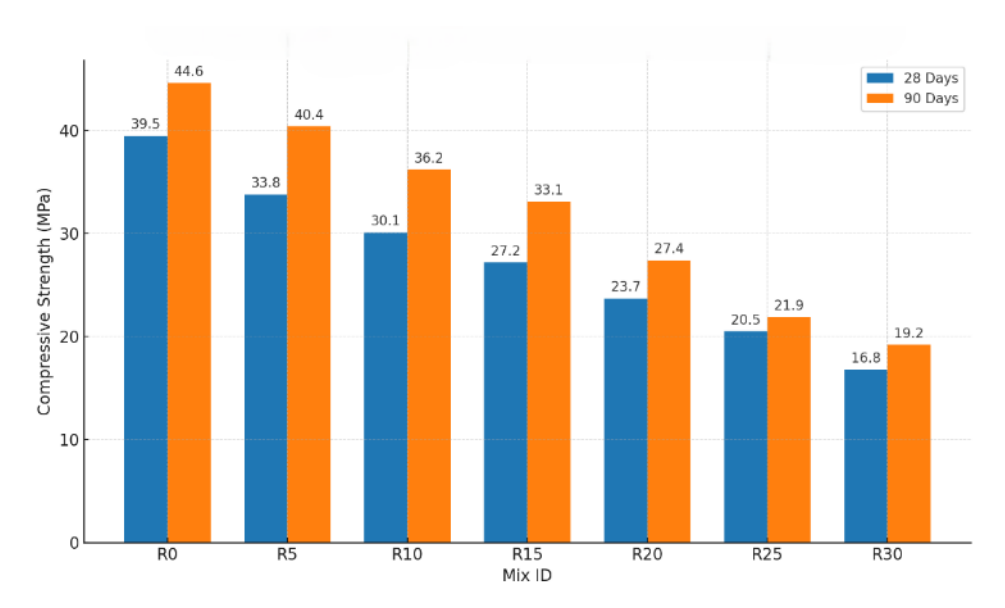


Fig. 5. Compressive strength test results

3.2. Elastic Modulus

Table. 4 presents the average values of the elastic modulus at 28 days. this property consistently decreases with increasing *GTR* replacement. Concrete mixes containing CR (*R5*, *R10*, *R15*, *R20*, *R25*, *and R30*) showed reductions in elastic modulus of approximately 8.5%, 15.4%, 21.6%,24.9%,30.9 and 37.9%respectively, compared to the reference mix (*R0*). This decline is mainly attributed to the inherently low stiffness of rubber particles and their weak interfacial bonding with the surrounding cementitious matrix, which compromises the concrete's resistance within the elastic range. Comparing the results across all mixtures reveals a clear inverse relationship between rubber content and elastic modulus higher replacement levels consistently led to lower stiffness. This trend is clearly illustrated in Fig. 6, which shows a steady degradation in elastic performance. These findings are in line with previous studies [43,44], which reported significant reductions in stiffness when rubber particles are incorporated, especially in lightweight concrete mixes.

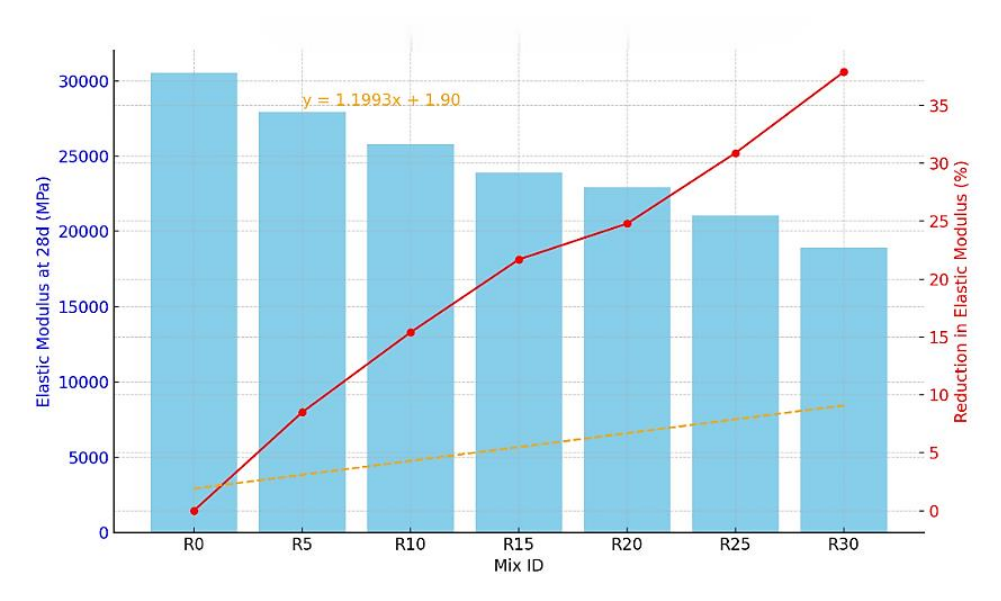


Fig. 6. Elastic modulus and reduction at 28 day

3.3 Stress-Strain Behavior

The stress–strain curves of the investigated mixes demonstrated a clear progression with increasing rubber content, as shown in Fig.7. The reference mix *R0*, representing lightweight concrete enhanced with *PVA* fibers and pozzolanic additives, displayed a sharply rising linear segment followed by a softening post-peak response characterized by moderate ductility. This behavior is largely attributed to the combined effects of *PVA* fibers, which help delay crack propagation and increase energy absorption, and the role of fly ash and silica fume in refining the cement matrix and improving interfacial bonding.

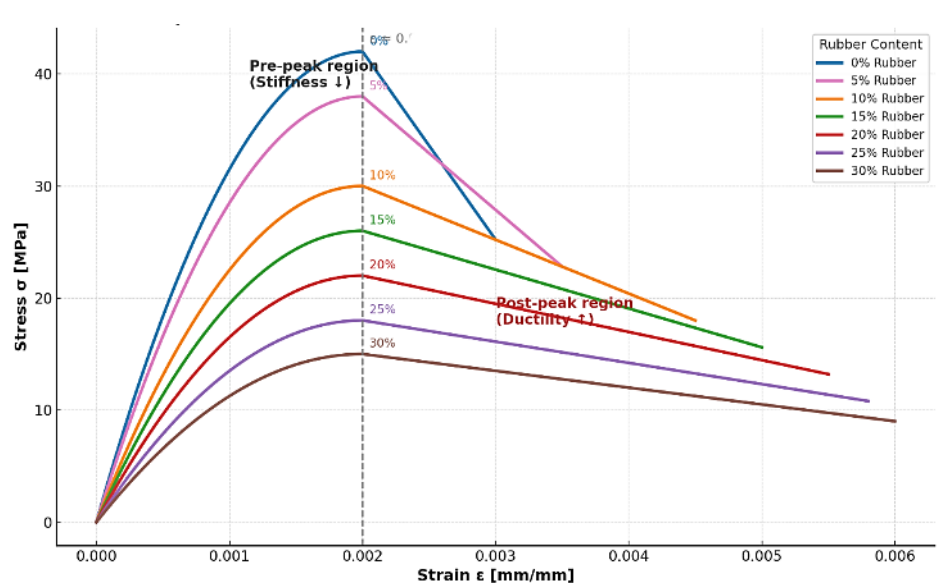


Fig. 7. Compressive stress-strain curves for reference concrete (R0) and rubberized concrete at 28 days

As outlined in Table 4, the recorded values for peak strain, ultimate strain, and peak stress align with the visual interpretations. A steady decline in peak compressive strength was observed as rubber content increased, while ultimate strain increased up to the *R10* mix before showing a reduction at higher replacement levels, indicating diminished ductility. As rubber content increased from *R5* to *R30*, a noticeable decrease in both peak strain and stiffness was evident, along with a steeper descending slope in the post-peak region most prominent in mixes *R25* and *R30*. This trend highlights a progressive weakening in structural integrity due to poor bonding between rubber

particles and the cementitious matrix, even though rubber inclusion contributed to greater deformability [45]. These observations are in agreement with previous research by [46-49], which similarly found that the introduction of rubber into fiber-reinforced concrete results in a more ductile but less rigid compressive behavior.

3.4 Flexural Strength Behavior

The flexural strength at 28 days of the lightweight fiber-reinforced concrete mixes incorporating rubber exhibited a consistent decline as natural sand was progressively substituted with GTR, as depicted in Fig.8a, and summarized in Table 4. The control mix (R0) achieved 4.72 MPa, while mixes R5, R10, R15, R20, R25, and R30 recorded 4.45, 4.13, 3.25, 2.88, 2.58, and 2.24 MPa, respectively. With increasing rubber content from 5% to 30%, the strength reduced incrementally by approximately 7.8%, 12.5%, 20.8%, 34.5%, 44.1%, and 52.5%, respectively, compared to the reference mix. This downward trend is primarily attributed to the elastic nature of rubber particles and their inadequate adhesion to the cementitious matrix, which weakens the ITZ and raises the likelihood of microcracking under flexural loads. Nonetheless, the incorporation of 2% PVA fibers significantly enhanced post-cracking tensile performance through crack-bridging action, while the addition of pozzolanic materials such as fly ash and silica fume contributed to refining the cement matrix microstructure. Concrete mixes with moderate rubber content (R5 to R15) demonstrated a favorable compromise between strength and ductility, making them suitable for lightweight structural elements where both mechanical strength and energy dissipation are required. As illustrated in Fig. 8b, mixes like R10 showed gradual and controlled crack propagation, reflecting improved post-cracking behavior due to the combined influence of fibers and rubber particles. These outcomes align with prior research by [50-52], which emphasized the advantages of fiber-rubber hybrid systems in enhancing flexural toughness and ductility in concrete applications

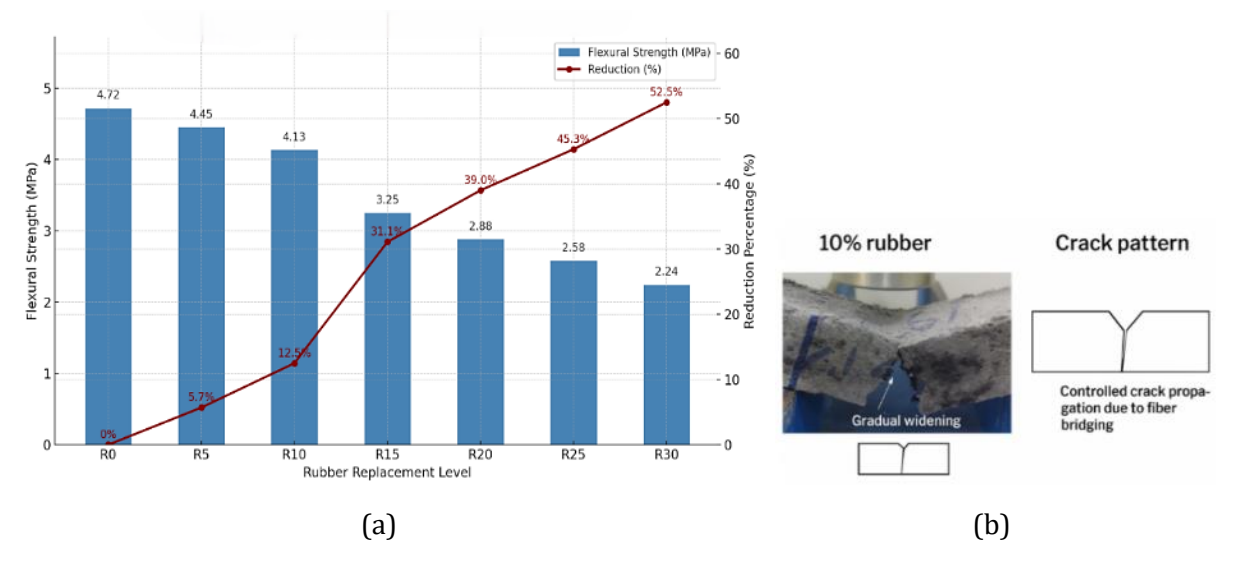


Fig. 8. (a) Flexural strength development of rubberized lightweight conrete and (b) crack pattern and fracture response of rubberized mortar under flexural loading

3.5 Interrelationship Between Physical Properties of Rubberized Lightweight Mortar

The integration of GTR into lightweight cementitious matrices significantly modifies their physical properties, particularly dry density, water absorption, and UPV . As shown in Fig.9, increasing the rubber content leads to a continuous decrease in dry density, primarily due to the low specific gravity of rubber granules (~ 1.10) compared to that of natural sand. This reduction in density is accompanied by a relative increase in water absorption, which is attributed to the rough and flexible surface of rubber particles that contribute to the formation of micro-voids within the cementitious matrix, thereby increasing overall porosity and disrupting the continuity of the internal concrete

structure. Parallel to this, UPV values also decline with increasing rubber replacement, reflecting a decrease in internal stiffness and homo-geneity caused by increased porosity [53,54]. To quantify the internal relationships between these variables, logarithmic regression models were applied. Dry density exhibited a strong inverse logarithmic relationship with water absorption, expressed by the model:

$$\rho = -501.32 \ln(WA) + 2496.73$$

Similarly, *UPV* was found to exhibit a comparable logarithmic decline as water absorption increased:

$$UPV = -1.83 \ln(WA) + 5.46$$
 11

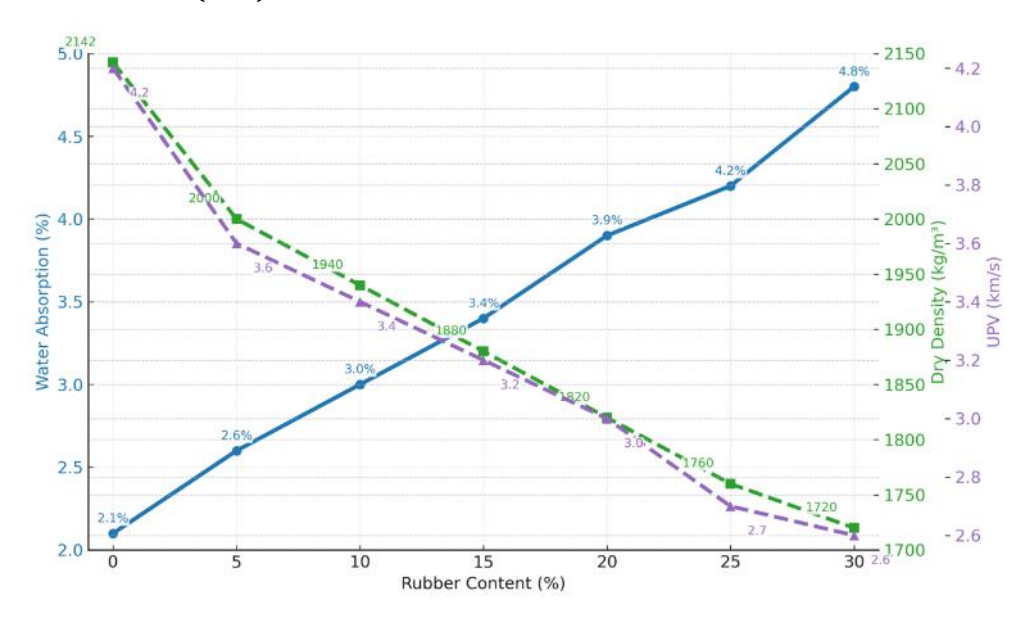


Fig. 9. Effect of rubber content on water absorption, dry density, and UPV at 28 days

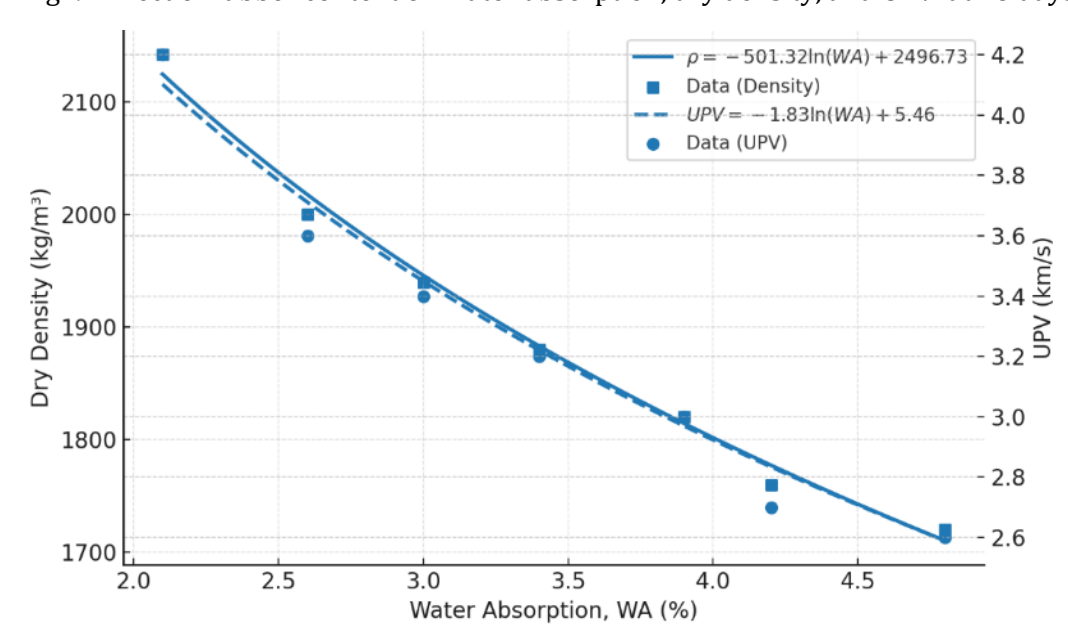


Fig. 10. Interrelationship between water absorption, dry density, and UPV

Both equations are depicted in (Fig.10) demonstrating high correlation coefficients ($R^2 > 0.98$), which indicates a strong interdependency among these physical parameters. Moreover, [55.56],

highlighted that the incorporation of mineral fillers and nano-sized pozzolans can refine the micro-structure and partially mitigate the permeability effects induced by rubber inclusion. Notably, the UPV and density values remained within the acceptable limits for lightweight structural concrete up to 15% rubber replacement, as per ASTM C330/C330M, supporting the feasibility of using such modified mortars in structural and semi-structural applications. The established correlations confirm that water absorption is not only a durability-related indicator but also a reliable proxy for estimating other physical characteristics in rubberized lightweight mortar systems.

3.6 Analytical Evaluation and Comparative Performance of the ANN in Predicting 28-Day Compressive Strength

An *ANN* model was developed to predict the 28-day compressive strength of lightweight rubberized concrete, achieving R^2 = 0.94, MSE = 0.72 MPa², and MAPE = 1.87%, confirming high predictive accuracy up to 30% rubber replacement. The parity plot Fig. 11 shows close agreement between predicted and experimental values along the 1:1 line, indicating reliable performance and practical utility in reducing repetitive tests and expediting mix design. A typical decreasing trend in f_(c 28d) with increasing rubber content is observed, mainly due to loss of matrix cohesion, the elastic/hydrophobic nature of rubber, and increased porosity that weakens the ITZ. A one-at-a-time perturbation sensitivity analysis was conducted: each input (GTR content, dry density, water absorption, and UPV) was perturbed slightly while the others were held constant. The resulting change in the predicted 28-day compressive strength f_(c 28d) was recorded and used to rank input influence; as shown in Fig. 12, UPV was the most influential input, followed by dry density and water absorption.

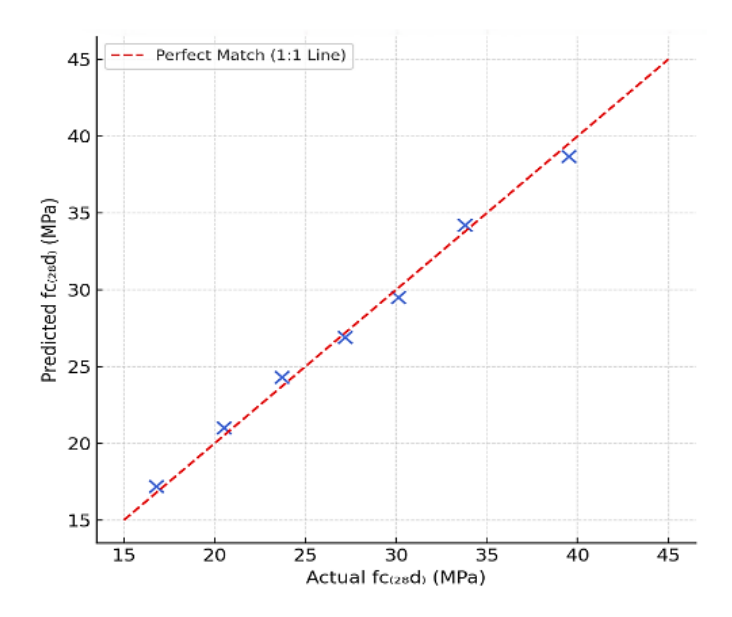


Fig. 11. Parity Plot: Predicted vs. Actual $f_{c \ 28d}$

Fig. 13 illustrates the joint effect of rubber content and UPV on $f_{c\ 28d}$: higher UPV combined with lower rubber content is generally associated with higher strength, highlighting the ANN's ability to capture nonlinear interactions. To further examine interrelationships, a Pearson correlation heatmap was constructed Fig. 14; its trends are consistent with the sensitivity ranking (rubber content negatively correlated with $f_{c\ 28d}$, UPV positively). Model accuracy and consistency were also verified through residual analysis (Fig. 15), where residuals are approximately normal and centered at zero, indicating unbiased predictions.

Table 4. Mechanical properties of rubberized lightweight mortar mixes (R0-R30)

						1.1.1.				7	
						Modulus	0.0015		(+2000)	Deformation at Peak	Flexural
	S	ompressi	Compressive Strength f_c	th f_c		Elasticity	reak co	reuk compressive stress s	Scress	Compressive	Strength
						Ec		smax		Stress	
										в	
Mix	Rubber	Mean	St. dev.	IOD	Reduction	Mean	Mean	St. dev.	LoD	Mean	Mean
ID	Content	f_{c28d}	[MPa]	%	[%]	$Ec[{ m MPa}]$	S_{max}	[MPa]	[%]	в	Flexural
	[%]	[MPa]					[MPa]				Strength 28d
											(MPa)
R0	0	39.5	1.86	4.71	0	30518.18	41.93	3.28	7.82	0.000141	4.72
R5	Ŋ	33.78	1.67	4.94	14.48	27927.84	37.94	2.9	7.64	0.000283	4.35
R10	10	30.12	1.21	4.03	23.75	25814.97	29.95	2.3	7.68	0.000424	4.13
R15	15	27.18	1.31	4.81	31.19	23907.16	25.96	1.95	7.51	0.00057	3.74
R20	20	23.7	1.12	4.71	40	22930.09	21.96	1.45	9.9	0.00070	3.1
R25	25	20.52	0.99	4.8	48.05	21083.51	17.97	1.38	7.67	0.00085	2.64
R30	30	16.79	0.94	5.61	57.49	18933.14	14.98	1.25	8.34	0.00097	2.24
Note:	Each mean v	alue was ca	Ilculated from	n three sp	secimens $(n = 3)$.	Standard deviat	tion (St. dev.)	and coefficien	t of variatio	Note: Each mean value was calculated from three specimens $(n = 3)$. Standard deviation $(St. dev.)$ and coefficient of variation (CoV) were computed accordinally	ted accordinaly

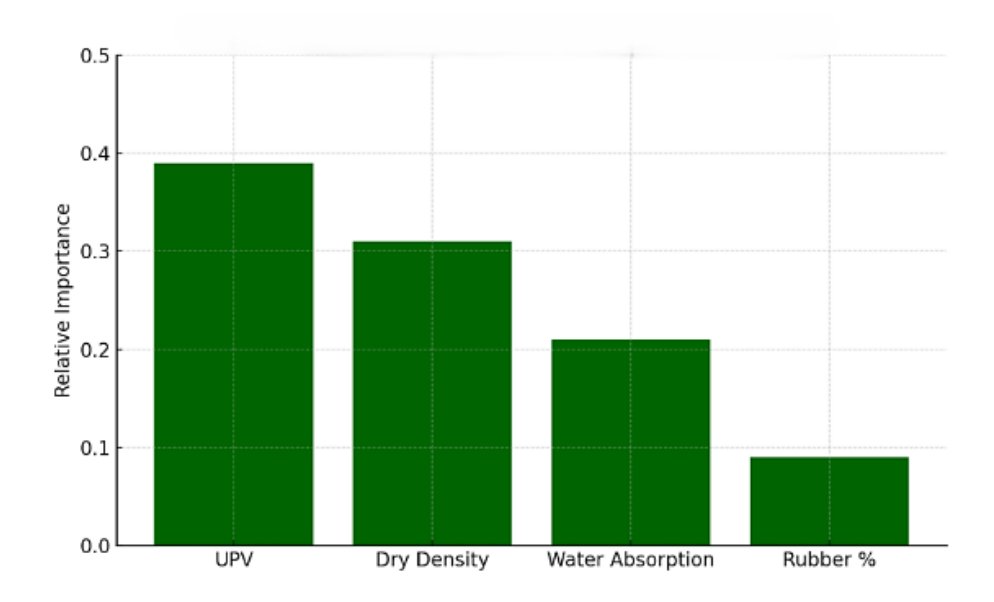


Fig. 12. Sensitivity Analysis of Inputs on $f_{c \ 28d}$

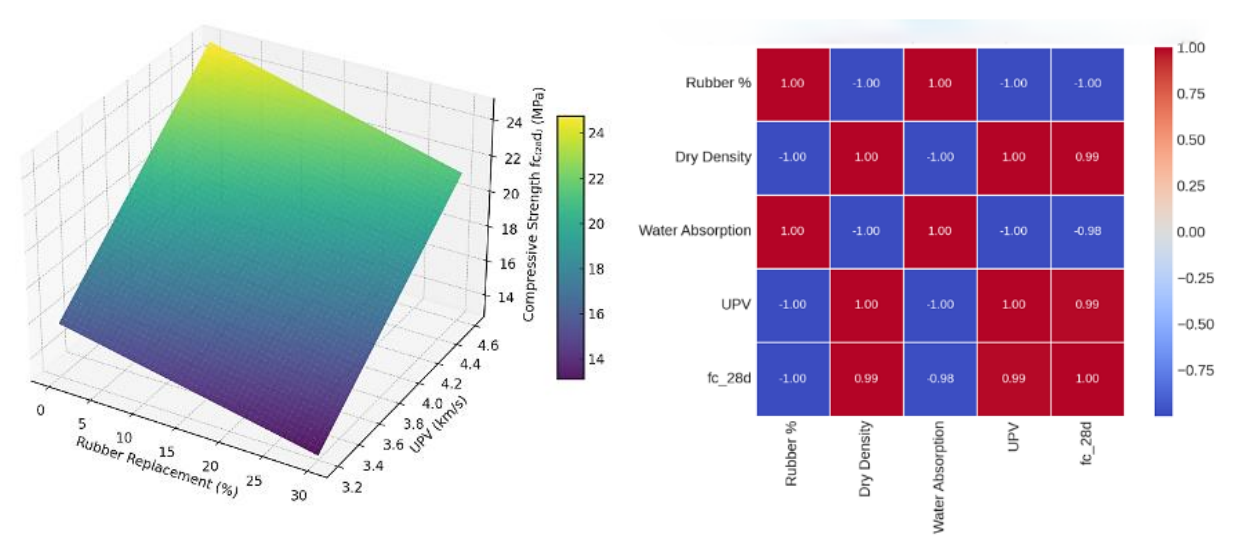


Fig. 13. Effect of rubber replacement (%) and UPV on 28-day compressive strength

Fig. 14. Correlation Heatmap Between Input Features and $f_{c,28d}$

For benchmarking, the ANN was compared with third-order polynomial regression, Gaussian Process Regression (*GPR*), and Support Vector Machines (*SVMs*). The SVM used a radial basis function kernel.

$$K(x_i, x_j) = exp(-\gamma \parallel x_i - x_j \parallel^2)$$
12

where γ controls the smoothness of the decision boundary and influences generalization. On the other hand, the *GPR* model employed a squared exponential covariance function:

$$k(x_i, x_j) = \sigma^2 exp\left(-\frac{\left(x_i - x_j\right)^2}{2l^2}\right)$$
13

The ANN outperformed the baselines (R² = 0.94; MSE = 0.72). Polynomial regression achieved R² = 0.85; MSE = 1.10 MPa²; GPR slightly exceeded SVM (R² \approx 0.84–0.86; MSE \approx 1.2–1.5 MPa²), while SVM (RBF) yielded R² \approx 0.82–0.83; MSE \approx 1.6–1.9. These results highlight the superiority of the ANN for rubberized lightweight concrete and align with previous studies [57–59]. The developed

ANN thereby offers a reliable, cost-effective tool for predicting the mechanical performance of sustainable concrete mixtures, enabling in-silico screening to reduce trial batches and shorten design cycles.

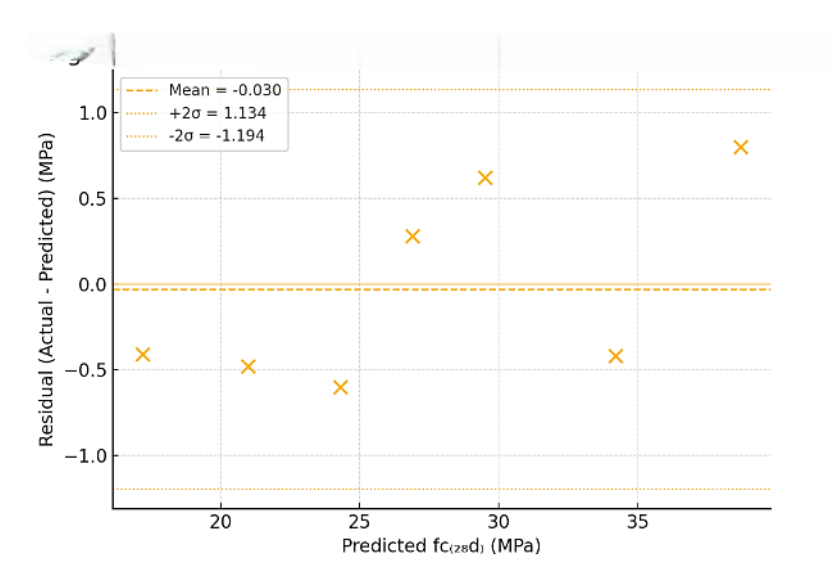


Fig. 15. Enhanced Residual Plot (with mean and $\pm 2\sigma$ bands)

4. Conclusions

These conclusions stem from a comprehensive set of advanced laboratory experiments and predictive modeling aimed at assessing the behavior of lightweight mortar containing recycled rubber. The evaluation focused on essential mechanical and physical characteristics, while also examining the effects of key parameters on structural performance through the application of artificial intelligence methods. The principal outcomes of the study are summarized below:

- Strength loss with rubber replacement. At 28 days, compressive strength decreased from 39.5 MPa (R0) to 16.8 MPa (R30) (-14.5%, -23.8%, -31.2%, -40.0%, -48.1%, -57.5% for R5-R30). At 90 days, strengths increased to 44.6 MPa (R0) and 19.2 MPa (R30), but the relative reductions remained 9.4–57.0%. The reduction is linked to ITZ weakening, higher porosity, and the elastic/hydrophobic nature of rubber
- Rubber-enhanced mixtures demonstrated increased deformability, as shown by stressstrain analysis and a notable reduction in elastic modulus reaching up to 37.9 %. Although flexural strength declined with greater rubber content, the presence of 2% PVA fibers enhanced tensile resistance after cracking, improved ductility, and boosted energy absorption capabilities.
- Density, UPV, and absorption. Dry density fell from ≈2140 to ≈1720 kg/m³ and UPV from ≈4.2 to ≈2.6 km/s as rubber increased from 0% to 30%, consistent with increased porosity and weaker internal continuity. Water absorption rose from ≈2.1% to ≈4.8%; using SCMs (fly ash, silica fume) with PVA fibers reduced pore connectivity and partially mitigated absorption.
- Peak strain showed a slight increase at moderate rubber levels before tapering off at higher replacement rates.
- Predictive modeling. The ANN predicted 28-day strength with R^2 = 0.94, MSE = 0.72 MPa², MAPE = 1.87%, outperforming polynomial regression, GPR, and SVM. Sensitivity analysis identified UPV as the most influential predictor of $f_{c\,28d}$, followed by dry density and water absorption.
- Semi-structural / non-critical structural uses: up to $\approx 15\%$ *GTR* is a practical upper bound in this work, giving $f_{c\ 28d}\approx 27\text{MPa}$, $f_{c\ 90d}\approx 33\text{MPa}$, $\rho\approx 1880\text{kg/m}^3$, $UPV\approx 3.2\text{km/s}$, and water absorption $\approx 3.4\%$. These mixes balanced reduced density with acceptable strength and UPV for light-duty elements and energy-dissipative applications.

- Non-structural uses (blocks, infill, pavements, vibration-control layers): 20-30% GTR produced $f_{c\ 28d}\approx24\rightarrow17$ MPa, UPV $\approx3.0\rightarrow2.6$ km/s, $\rho\approx1800\rightarrow1720$ kg/m³, and higher water absorption ($\approx3.9-4.8\%$). These are suited to non-load-bearing or serviceability-driven applications.
- Replacing a portion of natural sand with granulated tire rubber repurposes end-of-life tires and curbs the extraction of virgin aggregates. The lower unit weight further decreases structural self-weight and can translate into reduced transport and handling impacts.
- the ANN model provides a robust and efficient substitute for extensive experimental testing, offering valuable support for sustainable concrete design and optimization.

References

- [1] U.S. Tire Manufacturers Association (USTMA). Scrap Tire Management Summary. Washington (DC): USTMA; 2021. Available from: https://www.ustires.org
- [2] Rodezno O.O, Rodriguez J, Nazari M. Transforming waste to strength: Experimental study and performance evaluation of tire-derived aggregate concrete for sustainable building solutions. *Case Stud Constr Mater.* 2025;22:e04826. DOI:10.1016/j.cscm.2025.e04826.
- [3] Agrawal D, Ansari K, Waghe U, et al. Exploring the impact of pretreatment and particle size variation on properties of rubberized concrete. *Sci Rep.* 2025;15:11394. https://doi.org/10.1038/s41598-025-96402-v
- [4] Guo S, Dai Q, Si R, Sun X. Evaluation of properties and performance of rubber-modified concrete for recycling of waste scrap tire. *J Clean Prod.* 2017;148:681–93. https://doi.org/10.1016/j.jclepro.2017.02.046
- [5] Qader DN, Merie HD, Abdulhaleem KN. Impact of incorporating plastic fibers, walnut shells, and tire rubber fibers on the mechanical properties of concrete. *Electron J Struct Eng.* 2025. Available from: https://ejsei.com/EJSE/article/view/738
- [6] Majain N, Radin JM, Ahmad MH, Zainal SMI, Sulaiman MF. The mechanical properties of concrete waste slurry containing steel fiber and rubber powder. In: *Cutting-Edge Advances in Nanofibers and Fibers: Shaping Future Applications*. Hershey (PA): IGI Global; 2025. p. 24. DOI:10.4018/979-8-3373-0230-0.ch015
- [7] Makki OM. Heat influence on sustainable rubberized concrete mixes. *J Res Eng Struct Mater*. 2025. http://dx.doi.org/10.17515/resm2025-400ma0116rs
- [8] Imani DM. Optimization of cementitious concrete mix design containing various percentages of recycled tire rubber granules and reclaimed asphalt pavement (RAP). *J Trans Infrastruct Eng.* 2025. 10.22075/jtie.2025.37190.1720
- [9] Bheel N, Memon SA, Ali T, et al. Using optimization techniques on mechanical characteristics and sustainability assessment of rubberized concrete blended with PVA fiber through response surface methodology. *Int J CoCr Struct Mater.* 2024;18:59. https://doi.org/10.1186/s40069-024-00740-6
- [10] Drebin Z, Bensaid S, Laidoudi B. Comparative study of the lightening of concrete through the use of recycled tire rubber and expanded clay aggregate. *Slovak J Civ Eng.* 2023;31(2):16–24. https://doi.org/10.2478/sjce-2023-0009
- [11] Bušić R, et al. Recycled rubber as an aggregate replacement in self-compacting concrete—Literature overview. *Materials (Basel)*. 2018;11(9):1729. https://doi.org/10.3390/ma11091729
- [12] Thomas BS, Gupta RC, Kalla P, Csetenyi L. Strength, abrasion and permeation characteristics of cement concrete containing discarded rubber fine aggregates. *Constr Build Mater*. 2014;59:204–12. https://doi.org/10.1016/j.conbuildmat.2014.01.074
- [13] Thomas BS, Gupta RC, Panicker VJ. Recycling of waste tire rubber as aggregate in concrete: Durability-related performance. *J Clean Prod.* 2016;112:504–13. https://doi.org/10.1016/j.jclepro.2015.08.046
- [14] Liu J, Li J, Xu Y, Ma S. Mechanical properties of cement concrete with waste rubber powder. *Appl Sci.* 2024;14(15):6636. https://doi.org/10.3390/app14156636
- [15] Kashani A, Ngo T, Mendis P. Effects of surface treatments of recycled tyre crumb on cement–rubber bonding in concrete composite foam. *Constr Build Mater*. 2018;171:467–73. https://doi.org/10.1016/j.conbuildmat.2018.03.163
- [16] Kazmi SMS, Abbas S, Munir MJ, Khitab A, Javed MF. Application of waste tire rubber and recycled aggregates in concrete products: A new compression casting approach. *Resour Conserv Recycl.* 2021;167:105353. https://doi.org/10.1016/j.resconrec.2020.105353

- [17] Ince C, Shehata B, Derogar S, Ball R. Towards the development of sustainable concrete incorporating waste tyre rubbers: A long-term study of physical, mechanical & durability properties and environmental impact. *J Clean Prod.* 2021;334:130223. DOI:10.1016/j.jclepro.2021.130223
- [18] Islam MMU, Li J, Roychand R, Saberian M. A comprehensive review on the application of renewable waste tire rubbers and fibers in sustainable concrete. *J Clean Prod.* 2022;357:131836. DOI:10.1016/j.jclepro.2022.133998
- [19] Sheraz E, Ahmed A, Memon SA. Fresh and hardened properties of waste rubber tires-based concrete: A state of the art review. *SN Appl Sci.* 2023;5:119. https://doi.org/10.1007/s42452-023-05336-5
- [20] Kilani M, Beroual A, Younes R. Effect of crumb rubber (CR) on concrete's and mortar's structural properties: A review. *Iran J Sci Technol Trans Civ Eng.* 2024. https://doi.org/10.1007/s40996-024-01647-8
- [21] Karunarathna S, Linforth S, Kashani A, Liu X. Effect of recycled rubber aggregate size on fracture and other mechanical properties of structural concrete. *J Clean Prod.* 2021;313:127963. DOI:10.1016/j.jclepro.2021.128230
- [22] Medina NF, Hernández-Olivares F, Frías M. Durability of rubberized concrete with recycled steel fibers from tyre recycling in aggressive environments. *Constr Build Mater*. 2023;391:132619. https://doi.org/10.1016/j.conbuildmat.2023.132619
- [23] Liu J, Xu W, Li G, Chen B, Xiao Y, Huang H, Chen J. Performance and applications of polymer fiber rubber-reinforced concrete in civil engineering: A state-of-the-art review. *Polymers*. 2025;17(7):970. https://doi.org/10.3390/polym17070970
- [24] Rashid K, Yazdanbakhsh A, Rehman MU. Sustainable selection of concrete incorporating recycled tire aggregate to be used as medium to low strength material. *J Clean Prod.* 2019;224:396–410. https://doi.org/10.1016/j.jclepro.2019.03.197
- [25] Roychand R, Gravina RJ, Zhuge Y, Ma X. A comprehensive review on the mechanical properties of waste tire rubber concrete. *Constr Build Mater*. 2020;237:117651. https://doi.org/10.1016/j.conbuildmat.2019.117651
- [26] Han C, Pang J, Hu S, et al. Study on static and dynamic mechanical properties and microstructure of silica fume–polypropylene fiber modified rubber concrete. *Sci Rep.* 2024;14:12573. https://doi.org/10.1038/s41598-024-63341-z
- [27] Fu C, Li M. Frost resistance prediction for rubberized concrete based on artificial neural network. *Discov Appl Sci.* 2024;6:648. https://doi.org/10.1007/s42452-024-06357-4
- [28] Vadivel TS, Suseelan A, Karthick K, et al. Experimental investigation and machine learning prediction of mechanical properties of rubberized concrete for sustainable construction. *Sci Rep.* 2024;14:22725. https://doi.org/10.1038/s41598-024-73504-7
- [29] Bachir Rahali A, Mamoune Sidi Mohammed A, Trouzine H. Using artificial neural networks approach to estimate compressive strength for rubberized concrete. *Period Polytech Civ Eng.* 2018;62(4):858–65. https://doi.org/10.3311/PPci.11928
- [30] Hurukadli P, Parashar B, Shukla BK, Sharma P, Sihag S. Predictive modeling of crumb rubber-modified mortar: Insights from ANN, LR, RF, and M5P methods. *Asian J Civ Eng.* 2025. https://doi.org/10.1007/s42107-025-01270-6
- [31] Ly HB, Anh T, Mai HV, Van Quan T. Development of deep neural network model to predict the compressive strength of rubber concrete. *Constr Build Mater*. 2021;285:124081. https://doi.org/10.1016/j.conbuildmat.2021.124081
- [32] ASTM C330/C330M-14. Standard Specification for Lightweight Aggregates for Structural Concrete. West Conshohocken (PA): ASTM International; 2014.
- [33] ACI Committee 211. ACI 211.2-98: Standard Practice for Selecting Proportions for Structural Lightweight Concrete. Farmington Hills (MI): American Concrete Institute; 1998.
- [34] ASTM C109/C109M-21. Standard Test Method for Compressive Strength of Hydraulic Cement Mortars (Using 2-in. or [50-mm] Cube Specimens). West Conshohocken (PA): ASTM International; 2021.
- [35] ASTM C348-23. Standard Test Method for Flexural Strength of Hydraulic-Cement Mortars. West Conshohocken (PA): ASTM International; 2023.
- [36] ASTM C469/C469M-14. Standard Test Method for Static Modulus of Elasticity and Poisson's Ratio of Concrete in Compression. West Conshohocken (PA): ASTM International; 2014.

- [37] ASTM C597-22. Standard Test Method for Pulse Velocity Through Concrete. West Conshohocken (PA): ASTM International; 2022.
- [38] ASTM C642-21. Standard Test Method for Density, Absorption, and Voids in Hardened Concrete. West Conshohocken (PA): ASTM International; 2021.
- [39] Pham TM, Lee J, Pournasiri E, et al. Impact of rubber content on performance of ultra-high-performance rubberised concrete (UHPRuC). *Int J Concr Struct Mater*. 2024;18:59. https://doi.org/10.1186/s40069-024-00688-7
- [40] He S, Jiang Z, Chen H, Chen Z, Ding J, Deng H, Mosallam AS. Mechanical properties, durability, and structural applications of rubber concrete: A state-of-the-art review. *Sustainability*. 2023;15(11):8541. https://doi.org/10.3390/su15118541
- [41] Han C, Pang J, Hu S, et al. Study on static and dynamic mechanical properties and microstructure of silica fume–polypropylene fiber modified rubber concrete. *Sci Rep.* 2024;14:12573. https://doi.org/10.1038/s41598-024-63341-z
- [42] Stojanovic M, Šupić S, Jankovic K, Bojovic D, Terzić A, Malešev M. Investigation of the mechanical properties of concrete incorporating recycled rubber particles. *Sci Sintering*. 2024;56(1):27–27. https://doi.org/10.2298/SOS2405230275.
- [43] Jalal M, Nassir N, Jalal H. Waste tire rubber and pozzolans in concrete: A trade-off between cleaner production and mechanical properties in a greener concrete. *J Clean Prod.* 2019;238:117882. https://doi.org/10.1016/j.jclepro.2019.117882
- [44] Lv J, Zhou T, Du Q, Wu H. Effects of rubber particles on mechanical properties of lightweight aggregate concrete. *Constr Build Mater.* 2015;91:145–9. https://doi.org/10.1016/j.conbuildmat.2015.05.038
- [45] Eissa M, Habib A, Al Houri A, et al. Recent efforts on investigating the effects of recycled rubber content on the mechanical properties of structural concrete. *Discov Civ Eng.* 2024;1:16. https://doi.org/10.1007/s44290-024-00017-7
- [46] Chen X, Ge G, Zhou Y, Pan S, Ren A. The effects of high-content rubber and steel fibers on the workability and mechanical properties of concrete. *Compos Adv Mater*. 2025;34. https://doi.org/10.1177/26349833251343228
- [47] Strukar K, Kalman Šipoš T, Dokšanović T, Rodrigues H. Experimental study of rubberized concrete stress-strain behavior for improving constitutive models. *Materials*. 2018;11(11):2245. https://doi.org/10.3390/ma11112245
- [48] Liu L, Guan Q, Zhang L, Liu C, Cai X, Chen X. Evaluation of the stress–strain behavior of rubberized concrete under quasi-static compression. *J Mater Civ Eng.* 2022;34(11). https://doi.org/10.1061/(ASCE)MT.1943-5533.0004480
- [49] Walid M, Abdelrahman A, Kohail M, Moustafa A. Stress–strain behavior of rubberized concrete under compressive and flexural stresses. *J Build Eng.* 2022;59:105026. https://doi.org/10.1016/j.jobe.2022.105026
- [50] Yildiz S, Guneyisi E. Static and dynamic behavior of fiber-rubber modified cementitious materials. *Sci Rep.* 2024;14:12573. https://doi.org/10.1038/s41598-024-63341-z
- [51] El Naggar H, Abu Abdo AM. Properties and behavior of rubberized concrete enhanced with PVA fibers. *Buildings*. 2023;13(7):1681. https://doi.org/10.3390/buildings13071681
- [52] Ge J, Mubiana G, Gao X, Xiao Y, Du S. Research on static mechanical properties of high-performance rubber concrete. *Front Mater.* 2024;11:1426979. https://doi.org/10.3389/fmats.2024.1426979
- [53] Mohammed BS, Azmi NJ, Abdullahi M. Evaluation of rubbercrete based on ultrasonic pulse velocity and rebound hammer tests. *Constr Build Mater*. 2011;25(3):1388–97. https://doi.org/10.1016/j.conbuildmat.2010.09.004
- [54] Shi M, Jeong D, Lee S, Choi Y. Relationship between UPV and strength of rubber concrete. *Defect Diffus Forum*. 2018;382:225–9. https://doi.org/10.4028/www.scientific.net/DDF.382.225
- [55] Yasser N, Abdelrahman A, Kohail M, Moustafa A. Experimental investigation of durability properties of rubberized concrete. *Ain Shams Eng J.* 2023;14(6):102111. https://doi.org/10.1016/j.asej.2022.102111
- [56] Gupta T, Chaudhary S, Sharma RK. Assessment of mechanical and durability properties of concrete containing waste rubber tire as fine aggregate. *Constr Build Mater*. 2014;73:562–74. DOI:10.1016/j.conbuildmat.2014.09.102

- [57] Huang XY, Wu KY, Wang S, Lu T, Lu YF, Deng WC, Li HM. Compressive strength prediction of rubber concrete based on artificial neural network model with hybrid particle swarm optimization algorithm. *Materials*. 2022;15(11):3934. https://doi.org/10.3390/ma15113934
- [58] Hasanipanah M, Abdullah RA, Iqbal M, Ly HB. Predicting rubberized concrete compressive strength using machine learning: A feature importance and partial dependence analysis. *J Sci Transp Technol*. 2023;3(1):27–44. https://doi.org/10.58845/jstt.utt.2023.en.3.1.27-44
- [59] Choi Y, Kim IH, Lim HJ, Cho CG. Investigation of strength properties for concrete containing fine-rubber particles using UPV. *Materials (Basel)*. 2022;15(10):3452. https://doi.org/10.3390/ma15103452